Enhanced magnetopiezoelectric effect at the Néel temperature in CaMn_{2}Bi_{2}

Y. Shiomi, Y. Koike, N. Abe, H. Watanabe, and T. Arima

Phys. Rev. B **100**, 054424 — Published 19 August 2019

DOI: 10.1103/PhysRevB.100.054424

Enhanced Magnetopiezoelectric Effect at Néel temperature in $CaMn_2Bi_2$

Y. Shiomi[1], Y. Koike[2], N. Abe[2], H. Watanabe[3], and T. Arima[2]

[1] *Department of Basic Science, University of Tokyo, Meguro, Tokyo 153-8902, Japan*

[2] *Department of Advanced Materials Science, University of Tokyo, Kashiwa, 277-8561 Japan and*

[3] *Department of Physics, Kyoto University, Kyoto 606-8502, Japan*

(Dated: August 2, 2019)

Abstract

We have experimentally studied a magnetopiezoelectric effect (MPE), i.e. dynamic distortion caused by ac electric currents, in the antiferromagnetic conductor $CaMn_2Bi_2$ at low temperatures down to 77 K using laser Doppler vibrometry. When ac electric currents are applied to $CaMn_2Bi_2$, dynamic displacement signals which increase in proportion to the current amplitude are clearly observed at 77 K, but their magnitude and temperature dependence strongly depend on Joule heating effects caused by the applied electric currents. Especially, poor thermal contact of $CaMn_2Bi_2$ samples to the sample holder produces second-harmonic displacement signals owing to thermal expansion due to the Joule heating, and tends to affect the temperature dependence of the MPE signals. In a measurement run without any heating effects, a sharp enhancement of the MPE signal is observed at the Néel temperature of $CaMn_2Bi_2$, which suggests that fluctuations of itinerant Mn moments near the Néel temperature play an important role in the MPE. We speculate that electric currents produce nonequilibrium antiferromagnetic moments via the antiferromagnetic Edelstein effect and the induced antiferromagnetic momemts enhance the MPE signal with the help of a large magneto-volume coupling near the Néel temperature. The MPE efficiency as a piezoelectric response reaches 300 - 500 pC/N at a maximum, which is comparable to high values of piezoelectric coefficients detected in the piezoelectric (ferroelectric) ceramics.

I. Introduction

Low-symmetry materials have attracted great interest in condensed-matter physics for over a century. The breaking of spatial inversion symmetry in materials brings about many interesting electrical phenomena, such as switching of electric polarization [1–3] and piezoelectric responses [4–6]. On the other hand, the breaking of time reversal symmetry is essential in magnetic materials, and causes various magneto-optic [7] and magneto-transport [8] phenomena. These phenomena specific to magnetic materials can be controlled by the use of an external magnetic field, and their potential application has been studied intensively in the spintronics field [9].

In special materials in which both the spatial inversion and time reversal symmetries are broken, electric and magnetic properties are coupled [10]. The most pronounced phenomenon observed in these materials is a magnetoelectric effect [11, 12], where the magnetization (polarization) is controlled by electric (magnetic) fields. In the past two decades, multiferroic materials with ferroelectricity induced by magnetic order have received particular attention because of the relatively strong coupling between electric and magnetic order [13]. In the magnetic phase, magnetic order lowers the crystal symmetry and the resulting polar crystal symmetry allows for ferroelectricity. If the reduced crystal symmetry is noncentrosymmetric but nonpolar, spin-dependent piezoelectric effects are expected. A number of new spin-dependent piezoelectric effects have been explored in magnetic insulators, and generally termed piezomagnetoelectric effects [14–17].

Magnetopiezoelectric effect (MPE) [18–20], which refers to a linear strain response to electric currents and its inverse response in low-symmetric magnetic metals, is a generalization of magnetoelectric effects in insulators to metals [18]. In metallic materials with high conduction-electron densities, static (dc) piezoelectric responses are not allowed, even if the metals have a symmetry group low enough to support a static polarization. This is because the static surface charge density is screened out by bulk conduction electrons. However, it was recently proposed that dynamic distortion can arise in response to electric currents without screening effects in antiferromagnetic metals that simultaneously break time-reversal and spatial-inversion symmetries [19, 20]. The dynamical distortion is linear with the applied ac electric current, and the phase is the same between them. Microscopically, it was discussed that electric currents induce an electronic nematic order in metals lacking inversion

and time-reversal symmetries such as (Ba,K)Mn_2As_2 [19]; the nematic order accompanies the modulation of Fermi surfaces, which in turn leads to a structural deformation through electron-lattice couplings. On the other hand, Varjas *et al.* put forward a topological origin for the MPE [18]. Using a semiclassical formalism, they have shown that electric currents are generated by dynamical strain under external magnetic fields in itinerant chiral magnets [18].

Since electric currents are associated with electric fields according to Ohm's law, the MPE may be viewed as a kind of piezoelectric effects [19, 20]. However, the MPE is physically different from the conventional piezoelectric effect for the following reasons. First, the MPE is observed only in magnetically ordered states in contrast to the piezoelectric effect irrespective of magnetism, since the MPE requires the breaking of time reversal symmetry. Furthermore, the MPE requires electric conduction, and is not observed in magnetic insulators that do not conduct electricity. This obviously differentiates the MPE from the piezomagnetoelectric effect reported in insulating magnets [14–17]. Second, the electric field is an intrinsic quantity in the piezoelectric effect, while the electric current is intrinsic in the MPE. Varjas *et al.* proposed generation of pyroelectric currents in response to dynamical strain [18], while Watanabe *et al.* considered a non-equilibrium strain response to Ohmic currents accompanying Joule heating [19, 20]. Though a static strain can produce dc electric field or polarization in the piezoelectric effect, only a dynamic response is allowed in the MPE.

The MPE proposed by Watanabe *et al.* [19] was first experimentally demonstrated for the antiferromagnetic metal $EuMnBi_2$ by some of the present authors by measuring current-induced displacements with use of laser Doppler vibrometry [21]. $EuMnBi_2$ is a layered compound, where the conducting layers of Bi square net and the insulating magnetic layers consisting of Mn-Bi and Eu layers are spatially separated [22–26]. The transport property is quasi two-dimensional, and a quantum Hall effect is observed at the very low temperatures thanks to very high electron mobility in the c plane [23]. In the antiferromagnetic state of Mn sites, the magnetic order lowers the crystal symmetry and $EuMnBi_2$ possesses the D_{2d} symmetry [27, 28], which is the same as hole-doped $BaMn_2As_2$, a model material of the MPE [19]. Hence, the MPE is also expected to occur in $EuMnBi_2$ below the Néel temperature.

In the antiferromagnetic phase of $EuMnBi_2$ [19, 20], it is expected from the D_{2d} symmetry that the application of interlayer electric current induces MPE displacement signals along

an inplane direction. Consistent with the symmetry argument, dynamic displacements in response to ac electric currents applied along the c axis were experimentally observed in the a direction, but not in the c direction [21]. Furthermore, the generated in-plane displacement had linear dependence on the amplitude of the supplied electric current, as expected in the MPE. These results provide evidence of the emergence of MPE in $EuMnBi_2$.

The observed MPE signal decreases with increasing temperature [21], which is seemingly consistent with the theoretical proposal that the MPE response becomes smaller at higher temperatures with lower carrier mobilities [19]. However, the observed temperature dependence of the MPE signal in $EuMnBi_2$ in part disagrees with the expectation: since the MPE is associated with the symmetry breaking by magnetic order, the MPE signal is expected to emerge upon the antiferromagnetic transition. Experimentally [21], however, the MPE signal decreased rapidly with increasing temperature from 77 K and disappeared at approximately 200 K, which is much lower than the Néel temperature of $EuMnBi_2$ (314 K). The disappearance of the MPE signal above 200 K was attributed to the coherent-incoherent crossover of interlayer transport due to the very strong anisotropy in $EuMnBi_2$ [21]. Above 200 K, the interlayer incoherent transport in $EuMnBi_2$ is not dictated by the Fermi liquid theory and thus the MPE becomes undetectable. Hence, to study the temperature dependence of the MPE across the magnetic transition temperature, highly-anisotropic $EuMnBi_2$ is not suitable, and further study on another magnetic material is necessary.

In this paper, we experimentally study the MPE for the antiferromagnetic conductor $CaMn_2Bi_2$. $CaMn_2Bi_2$ is a trigonal material which consists of Bi-Mn bilayers and Ca layers [29], as illustrated in Fig. 1(a). Mn atoms form a corrugated honeycomb network in which every other atom is shifted perpendicular to the ab plane [30]. Measurements of magnetization and powder neutron diffraction revealed the antiferromagnetic order at $T_N = 150$ K [31]. The magnetic moments lie in the ab plane, and their magnitudes are estimated to be 3.85 μ_B [31]. The magnetic moment smaller than 5 μ_B expected from the high spin state is attributed to delocalization of one d electron per Mn atom, while the others are localized and give rise to the observed large magnetic moment [31]. The crystal symmetry of $CaMn_2Bi_2$ is centrosymmetric ($P\bar{3}m1$) at room temperature, but the symmetry is reduced to a noncentrosymmetric one by the antiferromagnetic order. In the antiferromagnetic state below $T_N = 150$ K, the magnetic space group is $C2/m'$, $C2'/m$, or $P\bar{1}'$ [31], depending on the directions of Mn moments in the ab plane. Because of the very low symmetry, the MPE

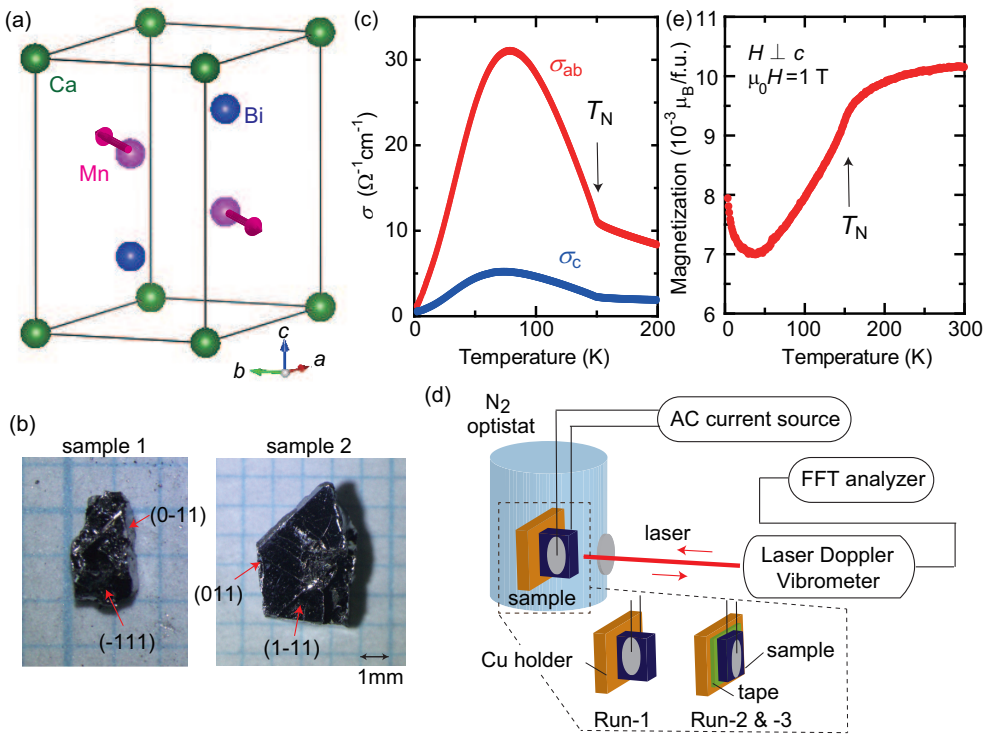

FIG. 1: (a) Schematic illustration of crystal structure for $CaMn_2Bi_2$, together with the magnetic structure of Mn ions below the antiferromagnetic transition temperature (T_N). (b) Photographs of Sample-1 and Sample-2 used for the measurement of the magnetopiezoelectric effect (MPE). (c) Temperature dependence of inplane conductivity σ_{ab} and interlayer conductivity σ_c for $CaMn_2Bi_2$. (d) Schematic illustration of the measurement setup for the MPE. (e) Temperature dependence of the magnetization measured in $\mu_0 H = 1$ T $\perp c$.

is expected in most crystal directions for $CaMn_2Bi_2$ [20]. Transport measurements show that $CaMn_2Bi_2$ is apparently metallic, but proposed to be a narrow gap (12-62 meV) semiconductor with a strong temperature dependence of the nominal Hall mobility [31]. Very recently, a large magnetoresistance was observed at very low temperatures below 20 K [29].

II. Method

Single crystals of $CaMn_2Bi_2$ were grown by a Bi-flux method following the literature [31]. Powders of Ca, Mn, and Bi were weighed to the molar ratio of Ca:Mn:Bi=1:2:10, and loaded in an alumina crucible. The crucible was sealed in a quartz tube in vacuum. The quartz tube was placed in a furnace, heated to 1000 °C, and held at that temperature for 48 hours. The quartz tube was then cooled slowly (2 °C/h) to 400 °C, where the excess Bi

flux was removed with the aid of a centrifuge. Many plate-like single crystals of $CaMn_2Bi_2$ with millimeter sizes were obtained. Two single-crystalline samples, whose photographs are shown in Fig. 1(b), were used in the MPE measurement. The dimensions of Sample-1 and Sample-2 were approximately $2 \times 2 \times 1$ mm^3 and $4 \times 3 \times 1$ mm^3, respectively.

For the MPE measurement, we used a laser Doppler vibrometer equipped with a liquid-nitrogen optistat for low-temperature measurements [21]. The laser Doppler vibrometry allows for non-contact detection of subpicometer-level tiny vibrations [32–35] by measuring the Doppler frequency shift of the scattered light from the sample using a two-beam laser interferometer. This technique has been widely used in room-temperature experiments for the characterization of piezoelectric thin films [34, 35] and for the detection of small cantilever oscillations with resonant frequencies [36]. Very recently, we applied the laser Doppler vibrometry to a low-temperature experiment, and successfully detected very small MPE signals in $EuMnBi_2$ at 77 K [21].

The setup of the MPE measurement is illustrated in Fig. 1(d). The $CaMn_2Bi_2$ sample (Sample-1 or Sample-2) was fixed on a Cu holder placed at the lowest part of the own-made sample rod, and then inserted into a liquid-nitrogen optistat. On the largest planes corresponding to the (-111) plane of Sample-1 and the (1-11) plane of Sample-2 [Fig. 1(b)], current electrodes were formed using conductive silver pastes, as illustrated in Fig. 1(d). Ac electric current with the constant amplitude in the range of 0-100 mA and the constant frequency in the range of 5 kHz-10 kHz was supplied to the samples using an ac current source (Model 6221, Tektronix, Inc.). Velocities of sample vibration showing up in response to applied electric currents were detected using the Doppler effect of red laser (wavelength of 633 nm) irradiated through a quartz window of the optistat. By combining the laser Doppler vibrometer with a fast Fourier transform (FFT) analyzer [32–35], we obtained a frequency spectrum of the vibration velocity of the sample. The obtained velocity was then numerically integrated with respect to time using the FFT analyzer, and finally the frequency dependence of the vibration amplitude of the sample was obtained. With an objective lens, the laser spot diameter was set to be less than 100 micron, which can be smaller than conventional domain sizes of bulk antiferromagnets [37].

Three MPE measurements have been run for two samples: Run-1 and Run-2 for Sample-1 and Run-3 for Sample-2 (see also Appendix A for further information). As illustrated in Fig. 1(d), the methods of fixing sample to the Cu sample holder are different between

Run-1 and Runs -2 and -3: in Run-1, the sample was fixed to the Cu holder using GE varnish; in Run-2 and Run-3, the sample was fixed on a thin insulating tape using silver paste (4922N, Du Pont) and also GE varnish. Note that, as shown in Appendix A (Fig. 6), the MPE signal is measured along different crystallographic directions in the different runs. Though the MPE coefficient is theoretically expected to have different magnitudes for different crystallographic directions, we have found that not the crystal direction but the method of fixing sample is mainly responsible for the measurement-run dependence of the experimental data, as discussed in the Results section.

III. Results

First, we show temperature dependence of conductivity in $CaMn_2Bi_2$. The conductivity is measured using a standard 4-terminal method with the electric current applied parallel and perpendicular to the *ab* plane: σ_{ab} and σ_c, respectively. The overall temperature dependence of the conductivity is in good agreement with previous reports [29, 31]. The magnitude of σ_{ab} at 300 K is $\sim 9\ \Omega^{-1}\mathrm{cm}^{-1}$, similar to that ($\sim 6\ \Omega^{-1}\mathrm{cm}^{-1}$) reported by Kawaguchi *et al.* [29]. As the temperature decreases from 300 K, the conductivity increases and shows a kink at 150 K. This kink in conductivity results from the reduction of magnetic scattering due to the antiferromagnetic order [31]. The observed metallic conductivity ($d\sigma/dT < 0$) in $CaMn_2Bi_2$ has been attributed to a strongly temperature dependent mobility rather than actual metallic behavior [31]. Though $CaMn_2Bi_2$ is a narrow-gap semiconductor, an increase in carrier mobility with decreasing temperature is stronger than the decrease in carrier concentration with decreasing temperature, and thus the metallic conductivity is observed in the wide temperature regime above 80 K. Below 80 K, the conductivity starts to decrease, which is a signature of semiconducting transport. Though $CaMn_2Bi_2$ hosts a layered structure, the anisotropy in electric transport is relatively small, and $\sigma_{ab}/\sigma_c \sim 5$.

We then performed measurements of the MPE for $CaMn_2Bi_2$. Figure 2 shows FFT spectra of displacements for $CaMn_2Bi_2$ samples at 77 K with and without application of ac electric currents. In general, background levels of displacement spectra obtained in the laser Doppler vibrometry tend to diverge at low frequencies. This is because numerical integral of sample vibration velocity with respect to time corresponds to the velocity divided by frequency; the obtained displacement is expected to increase with decreasing frequency f in proportion to

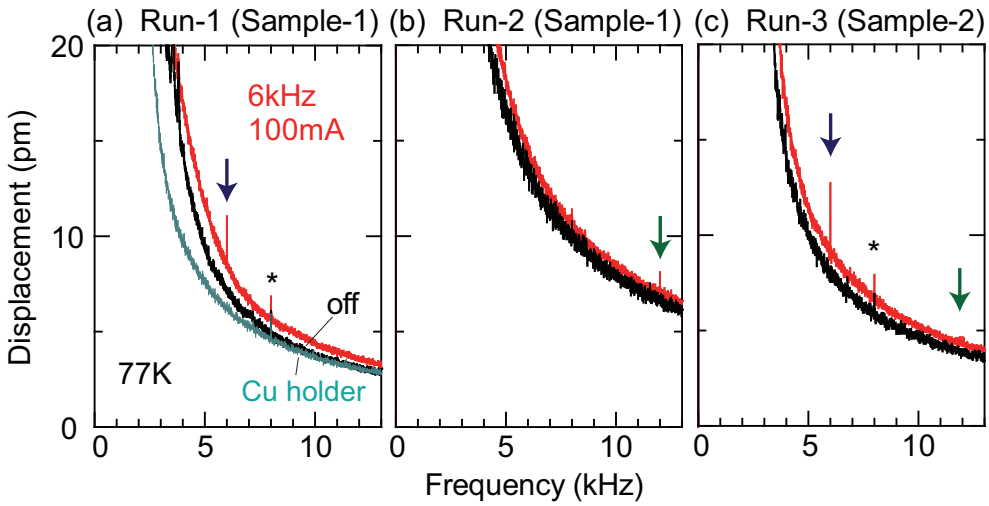

FIG. 2: Frequency dependence of displacement signals measured at 77 K with (red color) and without (black color) current application to $CaMn_2Bi_2$ samples. Here, the ac electric current of 6-kHz frequency and 100-mA amplitude (zero-to-peak amplitude) was applied along the [-111] direction of Sample-1 and the [1-11] direction of Sample-2. The displacement along the [0-11] direction was measured for Sample-1 in Run-1, along the [-111] direction for Sample-1 in Run-2, and along the [1-11] direction for Sample-2 in Run-3. See also Appendix A for the measurement configuration. The frequency of the electric current is indicated by the navy arrows, while the doubled frequency of the applied current is by green arrows. Asterisks at 8 kHz in (a) and (c) stand for extrinsic vibration from the sample rod; see text. In (a), a displacement spectrum of the Cu sample holder measured while 100-mA electric current is applied to the sample is also shown for the comparison (light green color).

$1/f$ as the background. Consistent with this expectation, the displacement spectra observed in $CaMn_2Bi_2$ exhibit approximately $1/f$ dependence in Fig. 2. Since background levels are smaller at higher frequencies, an electric current with a higher frequency is apparently better for the detection of current-induced displacement signals. However, it was reported that the MPE signals were also smaller at higher frequencies due to the non-ideal fixing of the sample to the Cu holder [21]; the back face of the sample was not stationary on the sample holder and could deform against the bonding material more significantly at higher frequencies. Hence, we selected 6 kHz as the typical frequency in the MPE measurement. In fact, as shown in Appendix B (Fig. 7), the MPE displacement signal decreased with increasing frequency, and was no longer observed at 10 kHz.

As shown in Fig. 2(a), when the ac electric current with 6-kHz frequency and 100-mA amplitude is applied to Sample-1 in Run-1, a displacement signal is found to appear at 6 kHz, the same frequency as the ac electric current. When the ac electric current is turned

off, the displacement signal at 6 kHz disappears, and hence can be attributed to the MPE signal. We also confirmed that the displacement signal at 6 kHz is irrelevant to vibrations of the Cu sample holder in Fig. 2(a). The magnitude of the observed MPE signal is ~ 11 pm, which is almost a half of that observed in $EuMnBi_2$ [21]. Note that at 8 kHz, a spike is also observed in the displacement spectra. However, the spike at 8 kHz is also observed in the current-off condition, and insensitive to electric currents, as well as temperature [Fig. 4(a)] and the current-frequency [Fig. 7]. The 8-kHz displacement signal is thereby ascribed to an artifact from the sample rod.

In Run-2 for Sample-1, by contrast, the MPE signal does not show up, even when the electric current of 100-mA amplitude is applied, as shown in Fig. 2(b). Instead, we found a clear second harmonic signal at 12 kHz in Fig. 2(b). This second harmonic signal indicates the presence of Joule heating effects in Run-2, since they should be proportional to the square of electric currents [$\sim \sin^2(\omega t) = \{1-\cos(2\omega t)\}/2$ where $\omega/2\pi = 6$ kHz]. In fact, the rise in temperature of the sample due to the Joule heating can cause a volume change via thermal expansion and magnetostriction effects. The signal at 12 kHz is thereby explained by thermomechanical effects of the sample due to Joule heating effects.

The different frequency spectra of displacements between Run-1 [Fig. 2(a)] and Run-2 [Fig. 2(b)] are attributed to different setups of sample fixing. As illustrated in Fig. 1(d), in Run-1, Sample-1 is directly attached to the Cu holder using insulating varnish, while, in Run-2, using a silver paste and varnish with a thin tape to electrically insulate the sample from the holder. The poor thermal contact of the sample to the heat bath in Run-2 gives rise to a strong Joule heating effect. Since the MPE signal is very small, special care about good thermal contact is required for the detection of the MPE. Note that in the previous MPE experiments for $EuMnBi_2$ [21], second harmonic signals were not observed in the similar setup to Run-2 [Fig. 2 in [21]].

The importance of the thermal contact in the MPE measurement is also confirmed by the experimental result for Sample-2 in Run-3, as shown in Fig. 2(c). In Run-3, though the sample setup is the same as that in Run-2, the MPE displacement signal is clearly observed at 6 kHz. The signal magnitude (~ 13 pm) is similar to that in Run-1. The second harmonic signal due to Joule heating in Run-3 is found to be much smaller than that in Run-2, and practically negligible at 77 K. The smaller Joule heating effect in Run-3 than in Run-2 is attributed to a larger heat capacity of Sample-2 due to the larger sample volume of Sample-2

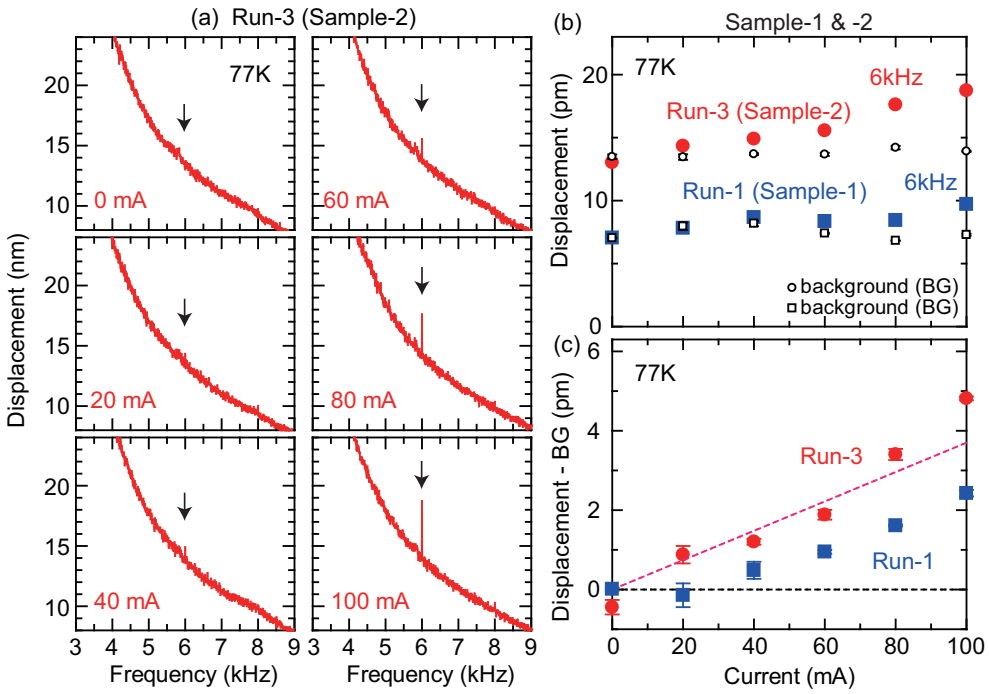

FIG. 3: (a) Frequency dependence of the displacement signals measured with various current amplitudes at 77 K in Run-3. Here, the electric current of 6-kHz frequency (denoted by black arrows) was applied to Sample-2. (b) The current-amplitude dependence of the displacement at 6 kHz and the background level for Run-1 and Run-3. The background levels (black open circles and squares) correspond to the averaged displacements around 6 kHz without current application. (c) The current-amplitude dependence of the displacement minus the background level in Run-1 and Run-3. The dotted lines are guides for eyes. See also Fig. 8 in Appendix C.

than that of Sample-1.

In Fig. 3, the magnitude of the MPE signal at 6 kHz is studied with different electric-current amplitudes. In Fig. 3(a), the frequency dependence of the displacement signal is shown for Run-3, when the current amplitude is changed from 0 mA to 100 mA. As the electric current increases, the MPE displacement induced by the 6-kHz electric current increases monotonically. Though the generated MPE signal is lower than the background level at 20 mA, the clear MPE signal is visible for the current amplitude higher than 40 mA.

The current-amplitude dependence of the MPE displacement at 6 kHz is summarized in Fig. 3(b). Here, the experimental results for Run-1 and for Run-3 are shown. While the background level near 6 kHz is almost constant for the whole data set in Run-3 as shown in Fig. 3(a), the background level varies largely with the electric-current amplitude in Run-1. At low temperatures, it is rather difficult to keep stable background levels, and

the background level often changes largely with time. To discuss appropriately the change of the current-induced signal with the electric current amplitude, temporal change of the background level needs to be taken into account.

The difference between the current-induced displacement signal and the background level is plotted against the electric current amplitude in Fig. 3(c). In both Run-1 and Run-3, the current-induced contribution is found to increase in proportion to the current amplitude, in agreement with the theoretical prediction of the MPE. See also Appendix C (Fig. 8). The proportionality coefficients are similar in magnitude for Run-1 and Run-3, and approximately 0.04 pm per milli-ampere. Note that the magnitude of the current-induced signal at 20 mA in Run-1 is lower than the background level, and thus the difference between the displacement and the background level is almost zero.

Next, temperature dependence of the MPE across the Néel temperature (150 K) is studied. Temperature dependence of the MPE signal is informative, since it depends on transport, mechanical, and magnetic properties [21]. On the other hand, the precise measurement on the temperature dependence of the MPE signal is difficult in the present setup. One reason for the difficulty is that background levels in the MPE measurement inevitably change by temperature shift of the laser position, since the sample rod in the optistat shrinks at low temperatures. The other reason is that the MPE measurement is performed in multidomain states of $CaMn_2Bi_2$, since it is in general difficult to make single magnetic-domain states in antiferromagnetic metals. Antiferromagnetic domains can be arranged differently in different thermal cycles. The MPE signals are partly canceled by the contributions from different domains, and thereby the temperature dependence of the MPE signal can be different in different measurement runs. Also, the presence of domain walls could affect the electric transport, and lead to different temperature dependence of the MPE. However, the effect of domain wall scattering could be negligible in electric transport of bulk samples [38] especially at high temperatures where the scatterings to phonons and magnons are significant.

The MPE displacement signal at 6 kHz was investigated at some temperatures as shown in Fig. 4. In Fig. 4(a), the spectra of the displacements at selected temperatures are shown for Run-1. At 77 K, the clear displacement signal at 6 kHz is observed in response to the electric current, as already shown in Fig. 2(a). As the temperature increases from 77 K, the MPE displacement becomes larger, shows a maximum at 151 K ($\approx T_N$), and then decreases. Notably, the MPE signal shows a maximum around T_N, and a small signal remains above

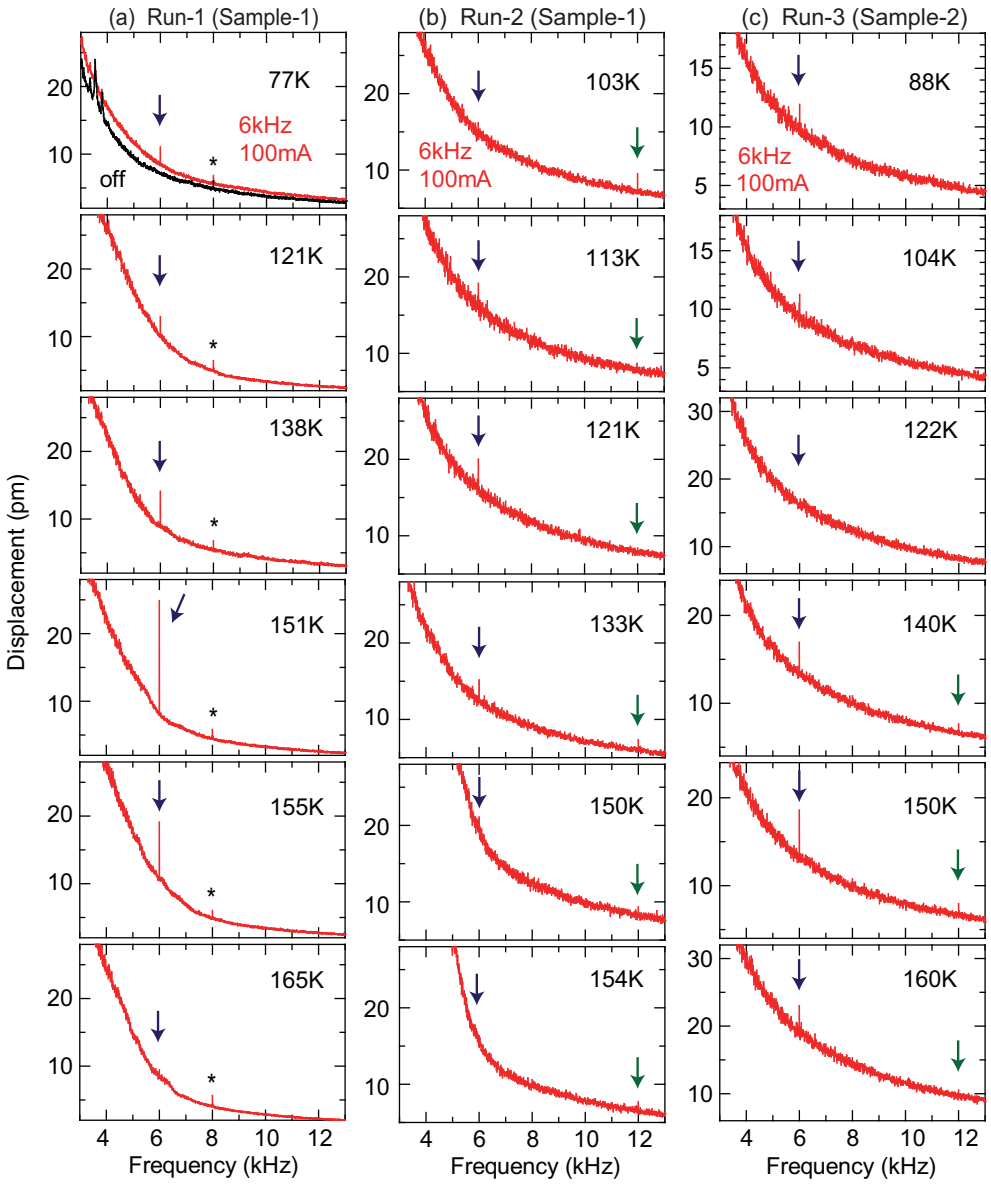

FIG. 4: Frequency dependence of the displacement at selected temperatures in (a) Run-1, (b) Run-2, and (c) Run-3. Here, the supplied electric current has the 6-kHz frequency and the 100 mA amplitude. The navy arrows indicate the frequency of the electric current (6 kHz), while the green arrows the frequency of the heating-induced displacement signals (12 kHz). Asterisks at 8 kHz in (a) stand for extrinsic vibration from the sample rod; see text.

T_N. At 165 K, the MPE displacement finally becomes lower than the background level. In the entire temperature regime, second harmonic signals were not observed.

In contrast to the experimental results in Run-1, the MPE signal is not observed at 77 K in Run-2, while the heating-induced signal appears at 12 kHz as shown in Fig. 2(b). Also at 103 K in Fig. 4(b), the MPE displacement signal is still indiscernible at 6 kHz in Run-2.

The Joule heating is significant also at 103 K, and clear heating-induced signal is observed at 12 kHz. At 113 K, the current-induced MPE displacement grows at 6 kHz, while the second-harmonic signal becomes small. Since the heat capacity of the sample and of the environment (such as bonding material and Cu holder) is larger at higher temperatures, the heating effect becomes less significant at higher temperatures. The heating-induced signals at 12 kHz are small and almost constant above 133 K, and even remain above T_N(= 150 K). The thermal impedance between the sample and the Cu holder should be insensitive to temperature, and likely to be mainly responsible for the second-harmonic signal observed in the high temperature regime. On the other hand, the MPE signal at 6 kHz shows a maximum at $\sim$ 121 K, and monotonically decreases to disappear above 150 K.

As shown in Fig. 4(c), the temperature dependence observed in Run-3 is more complicated. At 77 K, although the sample setup is the same as that in Run-2, the heating effect is less significant because of the larger heat capacity of Sample-2 than Sample-1, and the MPE signal is observed at 6 kHz as shown in Fig. 2(c). As the temperature increases from 77 K, the MPE displacement at 6 kHz decreases monotonically and disappears at 122 K. However, it then shows up again at 140 K. The MPE signal shows a maximum at 150 K, and decreases above T_N, similar to the temperature dependence in Run-1 [Fig. 4(a)]. As for the second harmonic signal at 12 kHz, it is observed only at high temperatures above 122 K. The magnitude of the second harmonic signal due to Joule heating is almost constant in the temperature regime, and similar to that in the same temperature regime in Run-2 [Fig. 4(b) and see also Fig. 5]. The thermal impedance between the sample and the Cu holder also seems a major issue in Run-3.

Temperature dependence of the displacement signals observed at 6 kHz (the current frequency) and also at 12 kHz are summarized in Fig. 5. Temperature dependences of the MPE signal and the background near 6 kHz are shown in the top row of Fig. 5. The background levels are the most stable with temperature in Run-1 among three runs, while they are rather scattered in Run-2 and Run-3. To discuss the temperature dependence of the amplitude of the current-induced signal in detail, the difference between the displacement signal at the current frequency and the background is plotted as a function of temperature in the middle row of Fig. 5. In Run-1 and Run-3, the signal tends to show a maximum at T_N, while monotonically decreases with increasing temperature toward T_N in Run-2. The different temperature dependence among three runs might be related with the different

crystal directions for the displacement measurement [Fig. 6], because the MPE coefficients are expected to have different magnitudes for different crystal directions. However, heating effects due to the poor thermal contact of the sample to the Cu holder is significant in Run-2 and Run-3 as already discussed, and should be mainly responsible for the different temperature dependence.

The magnitude of the second harmonic signal at 12 kHz due to the heating effect is plotted against temperature in the bottom row of Fig. 5. In Run-1, the heating-induced signal is not observed in the whole temperature range; this secures the reliability of the temperature dependence data of the MPE signals in Run-1. In contrast, in Run-2 and Run-3, the heating effects are observed appreciably. In Run-2, the second-harmonic signal is observed in the entire temperature range, and especially significant at low temperatures below 120 K where the MPE signal at 6 kHz is not observed. In Run-3, the second-harmonic signal is absent below 120 K, but appears above 120 K, at which the MPE signal once disappears [middle row in Fig. 5]. Hence, the temperature dependence of the current-induced MPE signal is dependent on that of the second-harmonic signal. Recall that the Joule heating effect induced by the 6-kHz electric current includes not only the second-harmonic contribution but also the frequency-independent one which can affect the 6-kHz signals via the rise of the sample temperature. However, quantitative discussion on the relation between the MPE signal and the heating-induced signal is elusive.

IV. Discussion

As shown in the Results section, the MPE response was clearly observed in $CaMn_2Bi_2$. An effective piezoelectric coefficient for the MPE in Run-1 is calculated by dividing the current-induced displacement by the electric field inside the sample. Using the electrode area ~ 4 mm^2, the electric current amplitude 100 mA, and a typical conductivity value 10 $\Omega^{-1}cm^{-1}$, the electric field inside Sample-1 is estimated to be 0.025 V/mm. Also, the maximum value of the current-induced stress observed at T_N is estimated to be 7.5 - 12.5 pm/mm by dividing the MPE displacement $\sim$ 25 pm ($\sim$ 15 pm if the background level is subtracted) by the sample thickness 2 mm. Hence, the effective piezoelectric coefficient is obtained as 300 - 500 pC/N at a maximum. At 77 K, it is about 50 - 200 pC/N. This magnitude is very large as a piezoelectric response and indeed comparable to the piezoelectric coefficients of alkaline

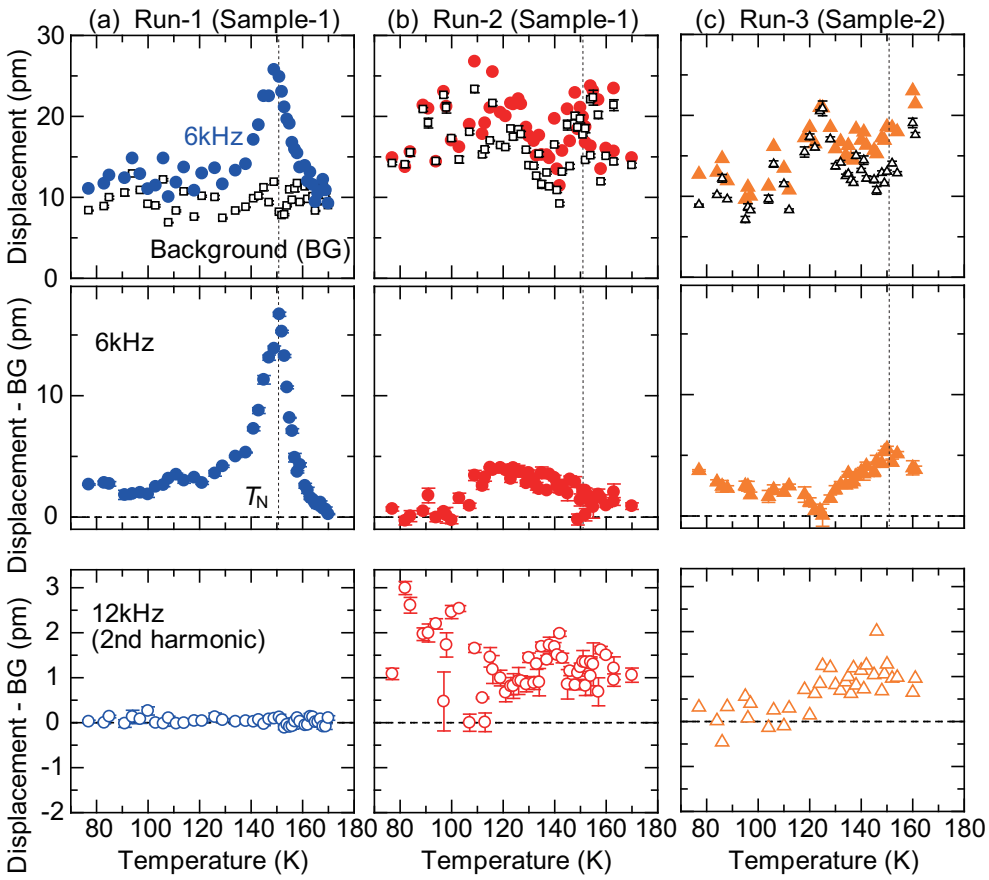

FIG. 5: Top row: Temperature dependence of the displacement signal measured at 6 kHz (closed symbols) in (a) Run-1, (b) Run-2, and (c) Run-3. Open symbols stand for background levels which are obtained by averaging displacements near 6 kHz. Middle row: Temperature dependence of the difference between the displacement signal at 6 kHz and the background level shown in top row in (a) Run-1, (b) Run-2, and (c) Run-3. Bottom row: Temperature dependence of the difference between the displacement signal at 12 kHz and the background level near 12 kHz. The data in Fig. 5 are taken from the temperature dependence of the displacements shown in Fig. 4.

niobates [39] and lead zirconate titanates [40]. The obtained piezoelectric coefficient, of which magnitude is too large to be attributed to the conventional piezoelectric effect that should be suppressed by the screening effect, can be ascribed to the MPE. Though the observed displacements in the MPE measurements are very small ($\sim$ pm) because of the very small magnitudes of the electric field (resistivity) inside $CaMn_2Bi_2$, potential performance of the MPE as the piezoelectric response is very high. Note that, in the previous MPE measurement for $EuMnBi_2$ [21], a very small value ($\sim$ 1 pC/N) of the MPE coefficient was reported. In this work [21], the set voltage value of a function generator (constant voltage source) was used for the estimation of the effective piezoelectric coefficient, whereas the set

current amplitude of a constant current source and the sample conductivity are used for a more accurate estimation of the electric field in the present experiment.

Though $CaMn_2Bi_2$ was reported to be a narrow-gap semiconductor [31], metallic-like conduction ($d\sigma/dT < 0$) is observed above $\sim$ 80 K [Fig. 1(c)] because of the enhanced mobility at low temperatures. The large mobility is favorable for the emergence of the MPE, since it has been theoretically proposed that the MPE coefficient is proportional to the scattering time [19]. On the other hand, the observed temperature dependence of the MPE signal (Fig. 5) is not simple: though the carrier mobility rapidly increases with decreasing temperature below T_N [31], the magnitude of the MPE signal does not change largely below T_N. Since the MPE is a Fermi-surface effect [19], the reduction of the carrier density at lower temperatures can also affect the temperature dependence of the MPE response.

The temperature dependent measurement (Figs. 4 and 5) has revealed that the MPE signal shows an anomaly at T_N in three measurement runs. Especially in Run-1 where the MPE measurement is not tainted by Joule heating effects, the temperature dependence of the MPE signal exhibits a sharp peak at T_N. The peak structure at T_N is partly reproduced in Run-3, though the Joule heating due to the poor thermal contact of the sample to the Cu holder is problematic in Run-3. The results clearly show that the current-induced displacement signal is related with the magnetic transition. The close relation between the displacement signals and the magnetic transition is again strong evidence of the MPE, since the conventional piezoelectric effect depends only on electrical properties and not on magnetic properties of materials. It is also noteworthy that, in the previous paper on the MPE for $EuMnBi_2$ ($T_N = 314$ K) [21], the temperature dependence of the MPE signal near the Néel temperature was not studied owing to the incoherent conduction above $\sim$ 200 K.

To the best of our knowledge, a linear strain response to electric currents in magnetic conductors is not known except for the MPE. Thermomechanical effects are not relevant with the strain response emerging at the current frequency, nor does magnetostriction respond to electric currents. Also, electromechanical or electrostrictive effects do not change due to the magnetic order. Hence, only the MPE has a potential to explain the experimentally observed phenomenon where the electric current, the antiferromagnetic order, and the lattice distortion are all coupled. Though the MPE is a generalization of magnetoelectric effects in insulators to metals [18], the temperature dependence of the MPE response is notably different from that of the magnetoelectric response; the magnetoelectric response develops

below T_N in line with the temperature evolution of the magnetic order parameter, while the MPE response tends to exhibit a peak at T_N [Fig. 5]. The peak structure at T_N indicates that spin fluctuations near T_N play an important role in the MPE, though the effect of spin fluctuations on the MPE was not discussed in the existing theory of the MPE [19]. It is well known that the spin fluctuation is rather essential in itinerant magnetic systems near magnetic transition temperature [41] relative to localized magnetic systems. Since one of five $3d$ electrons per Mn is delocalized in $CaMn_2Bi_2$, itinerant nature of Mn spins may be important in the MPE near T_N. Note that the temperature dependence of the magnetization in $CaMn_2Bi_2$ clearly deviates from a Curie-Weiss function above T_N [Fig. 1(e)], suggesting the presence of strong antiferromagnetic fluctuations above T_N. The critical behavior of the MPE near the magnetic transition temperature could be a distinct feature from the magnetoelectric [11, 12] and piezomagnetoelectric [14–17] responses in insulating magnets.

Critical enhancement of the current-induced antiferromagnetic moment at T_N could be responsible for the observed peak of the MPE signal at T_N. In $CaMn_2Bi_2$, the application of electric currents to $CaMn_2Bi_2$ also causes an antiferromagnetic Edelstein effect [42, 43]. Antiferromagnetic spin polarization of conducting electrons are induced by electric currents, which then leads to an antiferromagnetic polarization of localized spins through a spin exchange coupling between conduction and localized electrons. This effect was theoretically studied in a Kondo system, and it was shown that an antiferromagnetic polarization of localized spins diverges near the Néel temperature [42]. The induced antiferromagnetic moments coupled with spin-orbit coupling lead to a nematic modulation of Fermi surfaces that can enhance the MPE signal. Moreover, the large antiferromagnetic polarization induced near T_N could align the antiferromagnetic domains as reported in CuMnAs [44] and Mn_2Au [45]. Since the MPE response is canceled by different antiferromagnetic domains, the domain alignment can also enhance the MPE response of $CaMn_2Bi_2$ near T_N. Last but not least, the nonequilibrium antiferromagnetic moments induced by electric currents may point in different directions from the antiferromagnetic structure shown in Fig. 1(a). It is undeniable that the MPE coefficient has totally different magnitudes for different antiferromagnetic structures; the MPE signal due to the antiferromagnetc Edelstein effect could have a much larger magnitude near T_N than that from the antiferromagnetic structure shown in Fig. 1(a).

Furthermore, the slight change of antiferromagnetic moments could produce a large dis-

tortion around T_N because of the magneto-volume effect [46]. In itinerant magnets in which the magnetization mainly originates from the polarization of band electrons, it is known that thermal expansion tends to diverge at the magnetic transition temperature [47–50]. This effect is called a magneto-volume effect, and has been studied in various itinerant magnets [47–50]. It was theoretically proposed in the framework of the self-consistent renormalization theory [51, 52] that spin fluctuations near the magnetic transition temperature enhance the magneto-volume effect, as observed in MnSi [48], $Gd_{67}Ni_{33}$ [49], and β-$Mn_{1-x}M_x$ (M =Ru and Ir) [50]. Also in $CaMn_2Bi_2$, since part of $3d$ electrons of Mn are delocalized, large volume change could be expected in response to small magnetization change near T_N. The presence of this magnetovolume effect may be consistent with the fact that the decrease rate of the MPE signal above T_N in Run-1 is exponential [Fig. 5(a)], while the enhanced factor of the antiferromagnetic Edelstein effect near T_N was proposed to follow a Curie-Weiss function [42]. Hence, the enhanced MPE observed near T_N in $CaMn_2Bi_2$ is explained by two effects enhanced due to spin fluctuations near the magnetic transition temperature: the antiferromagnetic Edelstein effect and the magneto-volume effect.

V. Conclusion

In summary, the MPE has been experimentally demonstrated for the antiferromagnetic conductor $CaMn_2Bi_2$ using laser Doppler vibrometry at low temperatures. When ac currents were applied to the samples, MPE displacement signals whose magnitudes increases in proportion to the applied current amplitudes were observed at 77 K. The magnitude of the displacement signals is very small ($\sim$ pm), but if we estimate an effective piezoelectric coefficient for the MPE of $CaMn_2Bi_2$, its maximum value reaches 300 - 500 pC/N being comparable to high values of piezoelectric coefficients detected in conventional piezoelectric materials, thanks to the very small electric field inside the sample due to the very high conductivity. We found that the MPE signal is susceptible to Joule heating of the sample, and thus the good thermal contact of the sample to the sample holder is required to discuss precisely the MPE signals. In fact, we showed that the temperature dependence of the MPE signal is related to that of the second harmonic signal caused by thermomechanial effects due to the Joule heating. In a measurement run without any heating-induced signals, the temperature dependence of the MPE signal shows a peak at the Néel temperature. The

peak structure at T_N is explained by critical enhancement of the antiferromagnetic Edelstein effect and the magneto-volume effect. Such an enhanced signal at T_N has not been observed in magnetoelectric effects or piezo-magnetoelectric effects in insulating magnets, and could be a distinct feature of the MPE unique in itinerant magnets.

Acknowledgement

The authors thank Y. Yanase, Y. Kuramoto, S. Shamoto, and M. Akatsu for fruitful discussions. This work was supported by JSPS (KAKENHI No. JP18H04215, No. 18H04311, No. 18H04309, No. 19H01835, No. 19K22124, and No. 19H02424). Y.S. was supported by JST ERATO Grant Number JPMJER1402, Japan, and H.W. was supported by JSPS through a research fellowship for young scientists (No. JP18J23115). The measurement of magnetization was performed using facilities of the Institute for Solid State Physics, the University of Tokyo.

Appendix A: Experimental configuration and sample pictures in the MPE measurement

In the MPE measurements, experimental configurations of sample setup are different among Run-1, Run-2, and Run-3; the setups are illustrated in Fig. 6(a). In Run-2 and Run-3, the direction of the electric current and the detection direction of the displacement are parallel, while not parallel in Run-1. As discussed in the main text, the different configurations between Run-1, Run-2, and Run-3 lead to different thermal contacts of the sample to the Cu sample holder, which results in different temperature dependence of the displacement in Figs. 4 and 5.

Appendix B: Dependence of the displacement signal on electric-current frequency at 77 K

In Fig. 7, the current-frequency dependence of the displacement signal is studied at 77 K in Run-1. Here, the amplitude of the electric current is fixed at 100 mA. When an electric current with the 5-kHz frequency is applied to the sample, the current-induced displacement

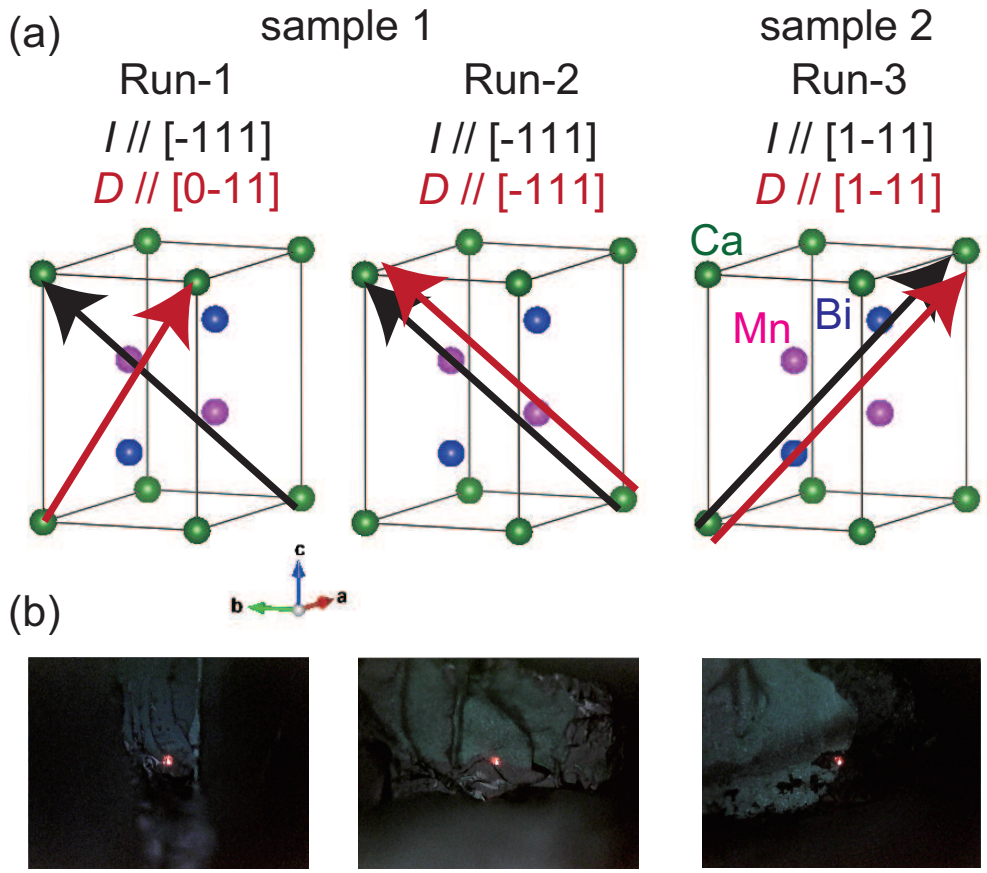

FIG. 6: (a) The relation between crystal directions and the directions of electric currents and displacements in the MPE measurements of Run-1, Run-2, and Run-3. (b) Photographs of the samples in the MPE measurements. The red dots correspond to spots of the lasers irradiated from the laser Doppler vibrometer.

signal is hard to recognize because of large background levels around 5 kHz. For the current frequencies of 6 kHz, 7 kHz, and 9 kHz, in contrast, the current-induced displacement signals are clearly observed. As the current frequency increases, the magnitude of the MPE displacement signal becomes smaller and finally disappears at 10 kHz. A similar frequency dependence of the MPE signal was reported in the previous paper for $EuMnBi_2$ [21], and explained in terms of non-ideal fixing of the sample to the Cu holder.

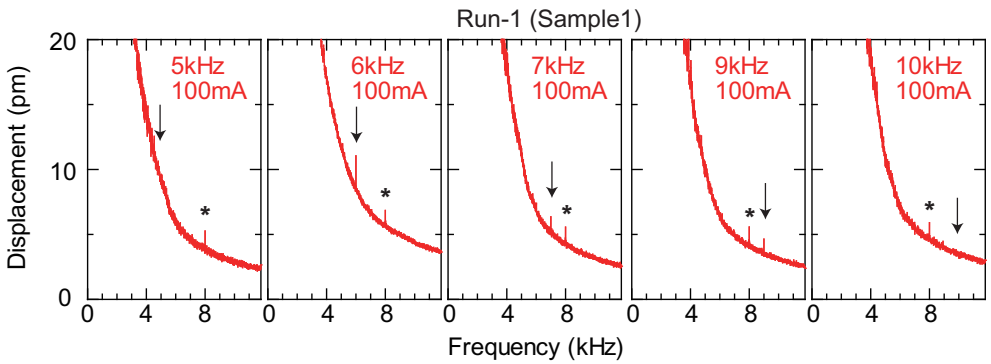

FIG. 7: Current-frequency dependence of the displacement signal at 77 K in Run-1. The current frequency is indicated by black arrows. The spikes at 8 kHz marked by asterisks are not changed by electric-current frequencies and attributed to extrinsic vibration from the sample holder; see also Fig. 2(a) where the spikes at 8 kHz are also observed without application of electric currents.

Appendix C: Dependence of the second-harmonic displacement signal on electric-current intensity at 77 K

In Fig. 8, we study the dependence of the second-harmonic displacement signal on the electric-current amplitude at 77 K in another measurement run. The used sample is Sample-2 and the experimental setup is the same as Run-3. The frequency spectra of the displacements around 6 kHz (the electric-current frequency) and 12 kHz (the doubled frequency) are shown in Figs. 8(a) and 8(b), respectively. In this measurement run, a second-harmonic displacement signal is observed at 100 mA in Fig. 8(b). While the current-induced displacement (the MPE signal) increases in proportion to the current amplitude as shown in Figs. 8(a) and 8(c), the current-amplitude dependence of the second-harmonic displacement is not simple; it is visible only at 100 mA in Fig. 8(b). In Fig. 8(c), we show the current-amplitude dependence of the magnitudes of the current-induced displacement (top row) and the second-harmonic displacement (bottom row). The MPE signals and the second-harmonic signals seem to have different current-amplitude dependence, though it is hard to study in detail the current-amplitude dependence of the second-harmonic signal within the measurement accuracy because of the relatively small magnitude of the second-harmonic signals.

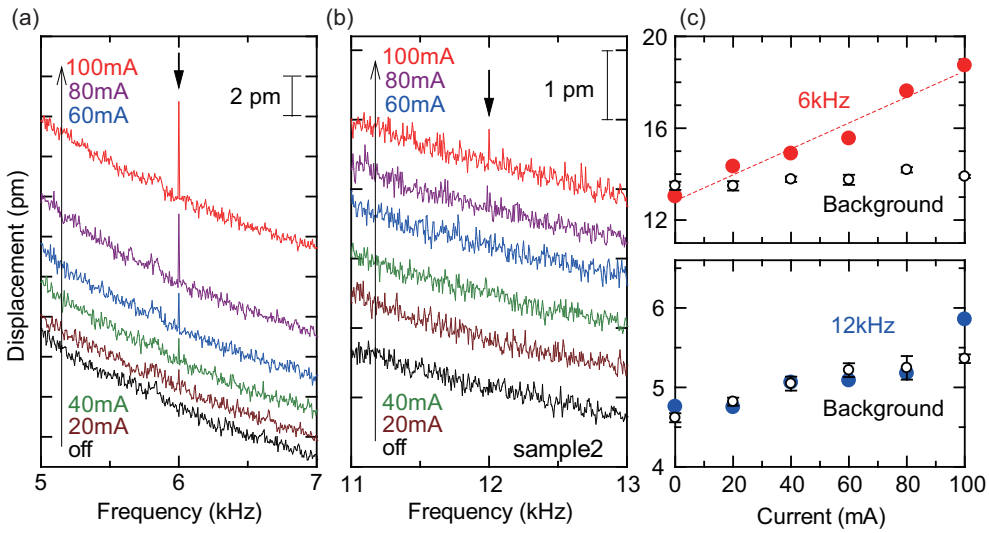

FIG. 8: (a),(b) Frequency dependence of the displacement at 77 K in another measurement run (a) around 6 kHz (the current frequency) and (b) around 12 kHz (the doubled frequency). The displacement spectra at different electric-current amplitudes are shown; here, each frequency-spectrum is shifted vertically for clarity. The arrows indicate the current-induced signal and the second-harmonic signal. (c) The current-amplitude dependence of the magnitudes of the current-induced displacement at 6 kHz (top row) and the heating-induced displacement at 12 kHz (bottom row). Background levels in the top (bottom) row are obtained by averaging displacements near 6 kHz (12 kHz) shown in (a) [(b)]. The dotted line in the top row is a guide for eyes.

[1] M. Dawber, K.M. Rabe, and J. F. Scott, Rev. Mod. Phys. 77, 1083 (2005).

[2] K. M. Rabe, M. Dawber, C. Lichtensteiger, C. H. Ahn, and J.-M. Triscone, *Physics of Ferroelectrics: A Modern Perspective* (Springer, Berlin, 2007).

[3] Ashim Kumar Bain and Prem Chand, *Ferroelectrics: Principles and Applications* (Wiley-VCH, Weinheim, 2017).

[4] Walter Heywang, Karl Lubitz, and Wolfram Wersing, *Piezoelectricity : evolution and future of a technology* (Springer-Verlag GmbH, Heidelberg, 2008).

[5] J. Tichý, J. Erhart, E. Kittinger, and J. Prívratská, *Fundamentals of Piezoelectric Sensorics: Mechanical, Dielectric, and Thermodynamical Properties of Piezoelectric Materials*, (Springer-Verlag GmbH, Berlin, 2010).

[6] D. Damjanovic, Rep. Prog. Phys. **61**, 1267 (1998).

[7] Taskeya Haider, Int. J. Appl. Electrom. **7** 17-24 (2017).

[8] N. Ashcroft, N. Mermin, D. Wei, *Solid State Physics: Revised Edition* (Cengage Learning Asia, Singapore, 2016).

[9] E. Y. Tsymbal and I. Zutic (Eds.), *Handbook of Spin Transport and Magnetism* (CRC Press, Boca Raton, 2011).

[10] W. Eerenstein, N. D. Mathur, and J. F. Scott, Nature **442**, 759-765 (2006).

[11] J.-P. Rivera, Eur. Phys. J. B **71**, 299-313 (2009).

[12] M. Fiebig, J. Phys. D: Appl. Phys. **38** R123-R152 (2005).

[13] T. Kimura, T. Goto, H. Shintani, K. Ishizaka, T. Arima, and Y. Tokura, Nature **426**, 55-58 (2003).

[14] T. Nakajima, Y. Tokunaga, Y. Taguchi, Y. Tokura, and T.-h. Arima, Phys. Rev. Lett. **115**, 197205 (2015).

[15] I. V. Bilych, K. R. Zhekov, T. N. Gaydamak, I. A. Gudim, G. A. Zvyagina, and V. D. Fil, Fiz. Nizk. Temp. **42**, 1419 (2016) [Low Temp. Phys. **42**, 1112 (2016)].

[16] T. N. Gaydamak, I. A. Gudim, G. A. Zvyagina, I. V. Bilych, N. G. Burma, K. R. Zhekov, and V. D. Fil, Phys. Rev. B **92**, 214428 (2015).

[17] V. D. Fil, M. P. Kolodyazhnaya, G. A. Zvyagina, I. V. Bilych, and K. R. Zhekov, Phys. Rev. B **96**, 180407(R) (2017).

[18] D. Varjas, A. G. Grushin, R. Ilan, and J. E. Moore, Phys. Rev. Lett. **117**, 257601 (2016).

[19] H. Watanabe and Y. Yanase, Phys. Rev. B **96**, 064432 (2017).

[20] H. Watanabe and Y. Yanase, Phys. Rev. B **98**, 245129 (2018).

[21] Y. Shiomi, H. Watanabe, H. Masuda, H. Takahashi, Y. Yanase, and S. Ishiwata, Phys. Rev. Lett. **122**, 127207 (2019).

[22] A. F. May, M. A. McGuire, and B. C. Sales, Phys. Rev. B **90**, 075109 (2014).

[23] H. Masuda *et al.* Sci. Adv. **2**, e1501117 (2016).

[24] H. Masuda, H. Sakai, M. Tokunaga, M. Ochi, H. Takahashi, K. Akiba, A. Miyake, K. Kuroki, Y. Tokura, and S. Ishiwata, Phys. Rev. B **98**, 161108(R) (2018).

[25] Y. Iwasaki and T. Morinari, J. Phys. Soc. Jpn. **87**, 033706 (2018).

[26] M. Chinotti, A. Pal, W. J. Ren, C. Petrovic, and L. Degiorgi, Phys. Rev. B **94**, 245101 (2016).

[27] Y. F. Guo, A. J. Princep, X. Zhang, P. Manuel, D. Khalyavin, I. I. Mazin, Y. G. Shi, and A. T. Boothroyd, Phys. Rev. B **90**, 075120 (2014).

[28] H. Masuda H. Sakai, H. Takahashi, Y. Yamasaki, A. Nakao, T. Moyoshi, H. Nakao, Y. Mu-

rakami, T. Arima, and S. Ishiwata, in preparation.

[29] N. Kawaguchi, T. Urata, T. Hatano, K. Iida, and H. Ikuta, Pys. Rev. B 97, 140403(R) (2018).

[30] D. E. McNally, J. W. Simonson, J. J. Kistner-Morris, G. J. Smith, J. E. Hassinger, L. DeBeer-Schmitt, A. I. Kolesnikov, I. A. Zaliznyak, and M. C. Aronson, Phys. Rev. B 91, 180407(R) (2015).

[31] Q. D. Gibson, H. Wu, T. Liang, M. N. Ali, N. P. Ong, Q. Huang, and R. J. Cava, Phys. Rev. B **91**, 085128 (2015).

[32] Y. Shiomi, T. Akiba, H. Takahashi, and S. Ishiwata, Adv. Electron. Mater. **4**, 1800174 (2018).

[33] R. Herdier, D. Jenkins, E. Dogheche, D. Rèmiens, and M. Sulc, Rev. Sci. Instrum. **77**, 093905 (2006).

[34] L. N. McCartney, L. Wright, M. G. Cain, J. Crain, G. J. Martyna, and D. M. Newns, J. Appl. Phys. **116**, 014104 (2014).

[35] S. Shetty, J. I. Yang, J. Stitt, and S. Trolier]McKinstry, J. Appl. Phys. **118**, 174104 (2015).

[36] Y.-J. Seo, K. Harii, R. Takahashi, H. Chudo, K. Oyanagi, Z. Qiu, T. Ono, Y. Shiomi, and E. Saitoh, Appl. Phys. Lett. **110**, 132409 (2017).

[37] M. Fiebig, D. Fröhlich, S. Leute, and R. V. Pisarev, J. Appl. Phys. **83**, 6560 (1998).

[38] W. Chen, L. Qian, and G. Xiao, Phys. Rev. B **98**, 174402 (2018).

[39] Y. Saito, H. Takao, T. Tani, T. Nonoyama, K. Takatori, T. Homma, T. Nagaya, and M. Nakamura, Nature (London) **432**, 84 (2004).

[40] P. K. Panda and B. Sahoo, Ferroelectrics **474**, 128 (2015).

[41] Tôru Moriya and Arisato Kawabata, J. Phys. Soc. Jpn. **34**, 639-651 (1973).

[42] Y. Yanase, J. Phys. Soc. Jpn. **83**, 014703 (2014).

[43] J. Železný, H. Gao, K. Výborný, J. Zemen, J. Mašek, Aurélien Manchon, J. Wunderlich, Jairo Sinova, and T. Jungwirth, Phys. Rev. Lett. **113**, 157201 (2014).

[44] P. Wadley *et al.* Science **351**, 587-590 (2016).

[45] S. Yu. Bodnar, L. Šmejkal, I. Turek, T. Jungwirth, O. Gomonay, J. Sinova, A. A. Sapozhnik, H.-J. Elmers, M. Kläui and M. Jourdan, Nat. Commun. **9**, 348 (2018).

[46] R. Weiss, Proc. Phys. Soc. **82**, 281 (1963).

[47] N. Martin, M. Deutsch, J.-P. Itié, J.-P. Rueff, U. K. Rössler, K. Koepernik, L. N. Fomicheva, A. V. Tsvyashchenko, and I. Mirebeau, Phys. Rev. B **93**, 214404 (2016).

[48] M. Matsunaga, Y. Ishikawa, and T. Nakajima, J. Phys. Soc. Jpn. **51**, 1153 (1982).

[49] Ikuo Nakai, Hatsuo Tange, Kensuke Konihsi, Tatsuo Kamimori, Akifumi Chikazawa, and Yasuhiro Motegi, J. Phys. Soc. Jpn. **72**, 1184 (2003).

[50] M. Miyakawa, R. Y. Umetsu, M. Ohta, A. Fujita, K. Fukamichi, and T. Hori, Phys. Rev. B **72**, 054420 (2005).

[51] T. Moriya and K. Usami, Solid State Commun., **34**, 95 (1980).

[52] Y. Takahashi and H. Nakano, J. Phys. Condens. Matter, **18**, 521 (2006).